J|A|C|S
ARTICLES
Published on Web 03/22/2002

Template Synthesis of Metal Nanowires Containing Monolayer Molecular Junctions

Jeremiah K. N. Mbindyo,[†] Thomas E. Mallouk,*[,†] James B. Mattzela,[‡] Irena Kratochvilova,[§] Baharak Razavi,[§] Thomas N. Jackson,[§] and Theresa S. Mayer[§]

Contribution from the Department of Chemistry, Intercollege Materials Program, and Department of Electrical Engineering, The Pennsylvania State University, University Park, Pennsylvania 16802

Received July 24, 2001

Abstract: Metal nanowires containing in-wire monolayer junctions of 16-mercaptohexanoic acid were made by replication of the pores of 70 nm diameter polycarbonate track etch membranes. Au was electrochemically deposited halfway through the 6 μm long pores and a self-assembled monolayer (SAM) of 16-mercaptohexadecanoic acid was adsorbed on top. A thin layer of Au was then electrolessly grown to form a metal cap separated from the bottom part of the wire by the SAM. Electron micrographs showed that the bottom and top metal segments were separated by an approximately 2 nm thick organic monolayer. Current−voltage measurements of individual nanowires confirmed that the organic monolayer could be contacted electrically on the top and bottom by the metal nanowire segments without introducing electrical short circuits that penetrate the monolayer. The values of the electrical properties for zero-bias resistance, current density, and breakdown field strength were within the ranges expected for a well-ordered alkanethiol SAM of this thickness.

Introduction

There is a growing interest in the use of molecules as functional components of nanoscale electronic circuits.[1−2] The very large increase in packing density that can be realized in molecule based electronic devices compared to present day silicon technology could result in substantial increases in computing power. There is also a growing realization that lithographic techniques are rapidly approaching practical technological limits.

Remarkable progress has been made in recent years in identifying candidate molecules with interesting electronic properties such as molecular conduction, rectification, negative differential resistance, and configurable switching.[4−15] These molecules can be used to perform logic and memory functions in electronic circuits, in a fashion analogous to the one currently performed by transistors. The broad variety of electronic functions available by synthetic modification of these molecules suggests many ways in which they may be used in hybrid or "post-silicon" applications. However, several key challenges still remain before these molecular devices can be used in practical circuits. First, there is need for a method that can be used to assemble molecular wires on surfaces, preferably in a deterministic manner. Most recent demonstrations of functional molecular devices have been done by using configurations such as e-beam defined nanopores or scanning probe tips, which are not readily compatible with existing microelectronic fabrication processes. Another challenge is to develop a method for rapid screening and electrical characterization of new candidate molecules. Addressing and fan out problems become increasingly severe as devices are scaled to molecular length scales. All these problems require techniques that can link the nanoscale world of molecules to the macroscopic world of conventional electronic circuits.

* Address correspondence to this author. E-mail: Tom@chem.psu.edu.
[†] Department of Chemistry.
[‡] Intercollege Materials Program.
[§] Department of Electrical Engineering.

(1) Bracht, H.; Nichols, S. P.; Walukiecwicz, W.; Silveira, J. P.; Briones, F.; Haller, E. E. *Nature* **2000**, *408*, 67−69.
(2) Carter, F. L., Ed. *Molecular Electronics Devices II*; Mercel Dekker: New York, 1987.
(3) Han, W.; Durantini, E. N.; Moore, T. A.; Moore, A. L.; Gust, D.; Rez, P.; Leatherman, G.; Seely, G. R.; Tao, N.; Lindsay, S. M. *J. Phys. Chem. B* **1997**, *101*, 10719.
(4) Bumm, L. A.; Arnold, J. J.; Dunbar, T. D.; Allara, D. L.; Weiss, P. S. *J. Phys. Chem. B* **1999**, *103*, 8122.
(5) Collier, C. P.; Mattersteig, G.; Wong, E. W.; Luo, Y.; Beverly, K.; Sampaio, J.; Raymo, F. M.; Stoddart, J. F.; Heath, J. R. *Science* **2000**, *289*, 1172.
(6) Balzani, V.; Credi, A.; Raymo, F. M.; Stoddart, J. F. *Angew. Chem., Int. Ed.* **2000**, *39*, 3349.
(7) Wong, E. W.; Collier, C. P.; Behloradsky, M.; Raymo, F. M.; Stoddart, J. F.; Heath, J. R. *J. Am. Chem. Soc.* **2000**, *122*, 5831.
(8) Xu, T.; Peterson, I. R.; Lakshmikantham, M. V.; Metzger, R. M. *Angew. Chem., Int. Ed.* **2001**, *40*, 1749.
(9) Metzger, R. M. *J. Mater. Chem.* **1999**, *9*, 2027.
(10) Metzger, R. M.; Chen, B.; Hopfner, U.; Lakshmikantham, M. V.; Vuillaume, D.; Kawai, T.; Wu, X. L.; Tachibana, H.; Hughes, T. V.; Sakurai, H.; Baldwin, J. W.; Hosch, C.; Cava, M. P.; Brehmer, L.; Ashwell, G. J. *J. Am. Chem. Soc.* **1997**, *119*, 10455.
(11) Metzger, R. M. *Acc. Chem. Res.* **1999**, *32*, 950.
(12) Asakawa, M.; Higuchi, M.; Mattersteig, G.; Nakamura, T.; Pease, A. R.; Raymo, F. M.; Shimizu, T.; Stoddart, J. F. *Adv. Mater.* **2000**, *12*, 1099.
(13) Collier, C. P.; Wong, E. W.; Belohradsky, M.; Raymo, F. M.; Stoddart, J. F.; Kuekes, P. J.; Williams, R. S.; Heath, J. R. *Science* **1999**, *285*, 391.
(14) Chen, J.; Reed, M. A.; Rawlett, A. M.; Tour, J. M. *Science* **1999**, *286*, 1550.
(15) Reed, M. A.; Zhou, C.; Muller, C. J.; Burgin, T. P.; Tour, J. M. *Science* **1997**, *278*, 252.

10.1021/ja016696t CCC: $22.00

One possible solution to these problems is to use nanowires as carriers of the electronically active molecules. Metal nanowires can be easily fabricated by several techniques. We and others have studied nanowires made by electrochemical template replication.[16−20] They can be nanoscopic in diameter but macroscopic in length. Therefore, it should be relatively easy to configure composites of nanowires and conducting molecules (molecular wires or electronically active molecules) in electronic circuits compared to wiring individual molecules.

Recently, we showed that DNA can be used to attach 200 nm diameter metal nanowires to Au surfaces[21] and demonstrated that nanowires can be modified with polymers by integrating them within and on the surface of the nanowire.[22] We have also developed a technique for aligning individual nanowires between lithographically patterned surfaces using an AC electric field.[23] In this paper, we report on the synthesis and characterization of 16-mercaptohexadecanoic acid molecular monolayer junctions embedded within 70 nm diameter metal nanowires. We show that electrical shorting of the monolayer can be prevented when forming the top metal contact by first depositing a metal cap on the carboxylate-terminated alkanethiol SAM using electroless seeding and plating prior to growing the top metal segment. For these junctions, the zero-bias resistance was found to exceed 10^{13} Ω, the high bias current was exponentially dependent on voltage, and the breakdown field strength was approximately 1.8×10^9 V/m. The critical bias for breakdown was also shown to degrade with successive cycling above the junction turn-on. These electrical properties are in good agreement with those measured using conductive probe atomic force microscopy (CP-AFM)[24,25] and mercury contacts[26] and establish that metal-molecule-metal nanowires synthesized following this procedure have the expected structural and electrical characteristics of alkanethiol monolayers. This work represents a significant step toward developing a new testbed to probe the electronic properties of electronically active molecules, as well as providing a possible route for integrating molecules into ultrahigh-density electronic circuits.

Experimental Section

Chemicals. Mercaptohexadecanoic acid was obtained from Aldrich Chemical Co. Au, Ag, and Ni electroplating solutions were obtained from Technic Inc. (RI).

Preparation of Nanowires. Prior to electrodeposition of the nanowires, one side of a 3.14 cm^2 track etched polycarbonate membrane (Osmonics) was first coated with a 100 nm layer of Au by thermal evaporation. This conductive layer seals the pores on one side of the membrane and serves as a cathode on which to electroplate metal. The membrane was then placed on a conductive Ag plate or an Au coated glass slide, such that the Au coated side was in contact with the conductive surface.

The electrochemical cell, which consisted of an 8 cm glass tube that terminated in a 3.14 cm^2 "O" ring seal, was placed on top of the membrane and held in place with a clamp. The electroplating solution was then added to the cell, and Au plated at a constant potential of −0.90 V vs SCE using a BAS 100 potentiostat. A saturated calomel electrode served as the reference electrode and a Pt wire as the counter electrode.

Assembly of SAMs. Monolayers of 16-mercaptohexadecanoic acid were assembled at the tip of the nanowires from 0.5 mM solutions in ethanol under an argon atmosphere for 24 h.

Electroless Plating of the Seed Metal. Electroless plating was done to introduce metal caps on top of the SAM.[27] Briefly, Sn(II) was first adsorbed on top of the monolayer from a 50:50 mixture of methanol and water acidified with 0.007 M trifluoroacetic acid. This adsorbed Sn(II) was then used to generate nanoparticles of Ag by adding ammoniacal $AgNO_3$ after thorough rinsing with methanol. To ensure the formation of a complete layer of metal on top of the monolayer, Au was electrolessly plated from a solution that was 0.04 M in Au(I) and contained formaldehyde as a reducing agent.

Plating of the Top Metal. The top portion of the nanowire was grown by using one of two methods. In the electroless plating method, the membrane was soaked in an Au electroless plating bath at 2 °C for 24 h. Any Au deposited on the outside of the membrane was removed by wiping with laboratory tissue paper, leaving the nanowires inside the pores. In the second method, the desired metal was deposited at constant potential from a plating bath until the pores were filled. The nanowires were then released by dissolving the membrane in dichloromethane.

Atomic Force Microscopy. The mechanism of the formation of capped monolayers was followed with AFM (Digital Instruments Nanoscope III). Since it is difficult to image inside the pores of the membrane with this technique, planar Au substrates were treated in the same manner as the nanowires and imaged at various steps in the process. The SAMs were grown on thermally evaporated Au from 0.5 mM ethanolic solutions.

X-ray Photoelectron Spectroscopy. Planar Au substrates were treated in the same way as Au nanowires, then analyzed on a Kratos Analytical XSAM 800 pci with a Mg 1253.6 eV X-ray source. The analysis was done at the Materials Research Laboratory, Pennsylvania State University.

I−V Characterization. Individual nanowires were positioned on an insulating substrate between lithographically defined electrodes using electrofluidic assembly. The substrate consisted of a 2 μm thick layer of SiO_2 that was grown by wet thermal oxidation of 1−10 Ω·cm n-type (100) silicon substrate (Addison Engineering, CA). A nonuniform alternating electric field was introduced in the dichloromethane by applying a 10−30 V_{rms}, 10 kHz voltage between a pair of 15 × 3000 μm interdigitated metal electrodes, which were defined by metal liftoff of 20 nm Ti and 100 nm Au deposited by thermal evaporation. The interdigitated metal electrodes were isolated electrically from the dichloromethane carrier fluid and an array of top metal alignment electrodes with a 300 nm thick layer of benzocyclobutane (BCB) (The Dow Chemical Company, MI) deposited by spin coating at 4000 rpm for 40 s and cured in a nitrogen atmosphere at 250 °C for 3 h. This dielectric layer was needed to prevent shorting of the interdigitated electrodes during nanowire alignment. Pairs of top metal alignment electrodes consisting of 10 nm Ti and 50 nm Au patterned by metal liftoff were deposited on top of the BCB such that one edge of each 150 × 350 μm^2 pad in the array overlapped the bottom metal electrodes

(16) Routkevitch, D.; Bigioni, T.; Moskovits, M.; Xu, J. M. *J. Phys. Chem.* **1996**, *100*, 14037.
(17) Martin, B. R.; Dermody, D. J.; Reiss, B. D.; Fang, M.; Lyon, L. A.; Natan, M. J.; Mallouk, T. E. *Adv. Mater.* **1999**, *11*, 1021.
(18) Xu, D.; Shi, X.; Guo, G.; Gui, L.; Tang, Y. *J. Phys. Chem. B* **2000**, *104*, 5061.
(19) Martin, C. R. *Science* **1994**, *266*, 1961.
(20) Foss, C. A.; Gabor, J.; Hornyak, L.; Stockert, J. A.; Martin, C. R. *J. Phys. Chem.* **1994**, *98*, 2963.
(21) Mbindyo, J. K. N.; Reiss, B. D.; Martin, B. R.; Keating, C. D.; Natan, M. J.; Mallouk, T. E. *Adv. Mater.* **2001**, *13*, 249.
(22) Yu, J.-S.; Kim, J. Y.; Lee, S. H.; Mbindyo, J. K. N.; Martin, B. R.; Mallouk, T. E. *Chem. Commun.* **2000**, *24*, 2445.
(23) Smith, P. A.; Nordquist, C. D.; Jackson, T. N.; Mayer, T. S.; Martin, B. R.; Mbindyo, J. K. N.; Mallouk, T. E. *Appl. Phys. Lett.* **2000**, *77*, 1399.
(24) Wold, D. J.; Frisbie, C. D. *J. Am. Chem. Soc.* **2001**, *123*, 5549.
(25) (a) Cui, X. D.; Zarate, X.; Tomfohr, J.; Sankey, O. F.; Primak, A.; Moore, A. L.; Moore, T. A.; Gust, D.; Harris, G.; Lindsay, S. M. *Nanotechnology* **2001**, *13*, 5. (b) Cui, X. D.; Primak, A.; Zarate, X.; Tomfohr, J.; Sankey, O. F.; Moore, A. L.; Moore, T. A.; Gust, D.; Harris, G.; Lindsay, S. M. *Science* **2001**, *294*, 571.
(26) Haag, R.; Rampi, M. A.; Holmlin, R. E.; Whitesides, G. M. *J. Am. Chem. Soc.* **1999**, *121*, 7895.
(27) Menon, V. P.; Martin, C. R. *Anal. Chem.* **1995**, *67*, 1920.

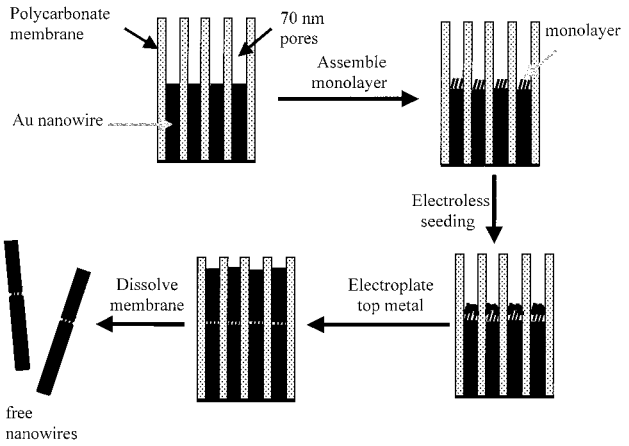

Figure 1. Synthetic scheme for the fabrication of bimetallic nanowires with in-wire monolayer junctions.

to provide a large capacitive coupling to the underlying biased electrode. Each large pad was connected to a 2×15 μm metal finger oriented such that adjacent fingers faced one another and had 3−5 μm gaps between their tips. These metal fingers concentrate the alternating electric field in the gap and also serve as the electrical contact to the nanowires.

Individual nanowires were aligned between the tips of the metal fingers by dispersing 10 μL of the nanowires suspended in dichloromethane on the surface of the substrate with the bias applied to the bottom interdigitated electrodes. The bias was maintained until the dichloromethane evaporated, which typically occurred in <1 min. The forces that induce alignment are due to nanowire polarization in response to the applied field,[23,28−32] and result in equal lengths of the nanowires contacting adjacent metal fingers. This also ensures that the nanowire molecular junctions are nearly centered in the gap between the metal fingers. Current−voltage measurements of individual metal and metal-molecule-metal nanowires were done at room temperature on an HP 4155 semiconductor parameter analyzer. Electrical contact was made to the large pads with a Micromanipulator 7000 probe station and low-noise coaxial probe holders, permitting measurement of sub-100 fA current levels.

Results and Discussion

Transmission Electron Microscopy (TEM) of Nanowires. The metal/SAM/metal nanowires were prepared by the steps shown in Figure 1. A monolayer of 16-mercaptohexadecanoic acid was first assembled at the tip of an electrochemically grown nanowire, and a seed metal layer was then deposited electrolessly on top of the monolayer.[27] The top half of the pore was filled by depositing more Au on top of the seed metal layer. Nanowires were obtained as a suspension in dichloromethane. Aliquots (5 μL) of this solution where mounted on microscope grids for imaging or aligned on lithographically patterned substrates for characterization of electrical properties.[23]

Figure 2a shows that the metal/SAM/metal junction can be imaged by using TEM. The image shows an Au/SAM/Au nanowire with an electrolessly grown top contact. In the electroless plating, Au(I) is reduced to Au(0) by formaldehyde. The junction can be identified as the place where the smooth electroplated Au meets the rough electrolessly deposited Au.

Figure 2b is a TEM image of a nanowire made by first adsorbing 16-mercaptohexadecanoic and then electroplating Ni

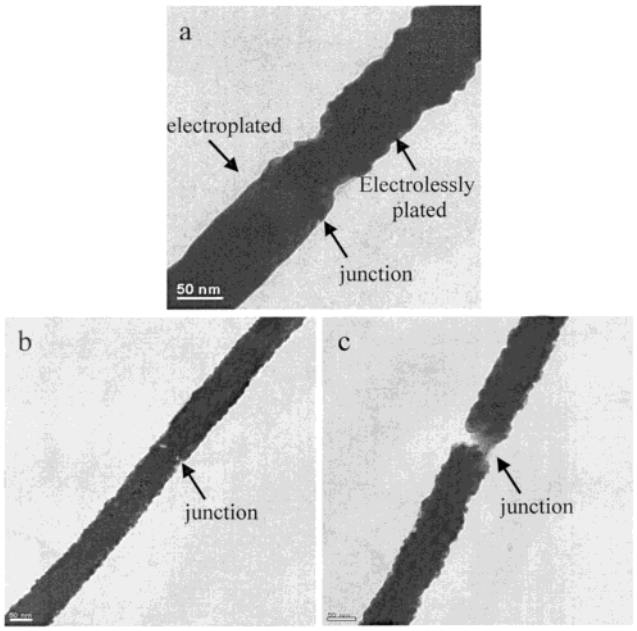

Figure 2. TEM images of (a) a nanowire with a 16-mercaptohexadecanoic acid SAM between two Au segments (the bottom half of the wire was electroplated and the top half was grown electrolessly), (b) a 16-mercaptohexadecanoic SAM junction between two electroplated segments of a nanowire; and (c) a nanowire with a 16-mercaptohexadecanoic SAM junction after 5 min in the electron beam.

on top. The second electroplating step was done after an electroless seed layer of Au was grown to block any pinholes. Again, the junction is clearly visible. In a close-up TEM view (×200K), there is a clear contrast between the metals and the molecular portions of the nanowire. The thickness of the SAM, estimated from the measured thickness of the low contrast area in the middle of Figure 2b, is approximately 2 nm. This is in good agreement with the value of 2.4 ± 0.1 nm found by ellipsometry for a monolayer self-assembled in the same way on a planar Au substrate, and in agreement with previously reported values.[33,34] It is possible to further enhance the contrast of the junction by exposing it to the electron beam in the TEM. As the intense electron beam hits the metal/SAM/metal interface, there is local heating. The metals begin to melt and the SAM decomposes, which clearly reveals the junction (Figure 2c).

We qualitatively established the formation of monolayers of the mercaptoalkanoic acids on the tips of the nanowire using cyclic voltammetry (CV) of ferrocyanide/ferricyanide couple. CVs were done in the same cell used for electroplating, with the nanowires still in the membrane. The oxidation/reduction current decreased by about 60% after adsorption of the SAMs. Because the wire tips act as an array of ultramicroelectrodes, giving sigmoidal cyclic voltammograms at a 100 mV/s scan rate, the fraction of the current remaining after SAM adsorption corresponds to the fraction of wires that contain defective SAMs. The CV data are consistent with electrical characterization data on individual nanowires (see below), which show 20−30% short-circuited devices.

Morphology of the Interface. Electron transport across the metal/SAM/metal interface can vary greatly depending on the

(28) Pohl, H. A. *J. Appl. Phys.* **1951**, *22*, 869.
(29) Pohl, H. A. *Dielectrophoresis*; Cambridge University Press: London, 1978.
(30) Roychowdhury, V. P.; Janes, D. B.; Bandyopadhyay, S. *Proc. IEEE* **1997**, *85*, 574.
(31) Service, R. *Science* **1999**, *286*, 2442.
(32) Hertel, T.; Martel, R.; Avouris, P. *J. Phys. Chem. B* **1998**, *102*, 910.
(33) Porter, M. D.; Bright, T. B.; Allara, D. L.; Chidsey, C. E. D. *J. Am. Chem. Soc.* **1987**, *109*, 3559.
(34) Sundar, V. A.; Liedberg, B.; Allara, D. L. *Langmuir* **1995**, *11*, 3882.

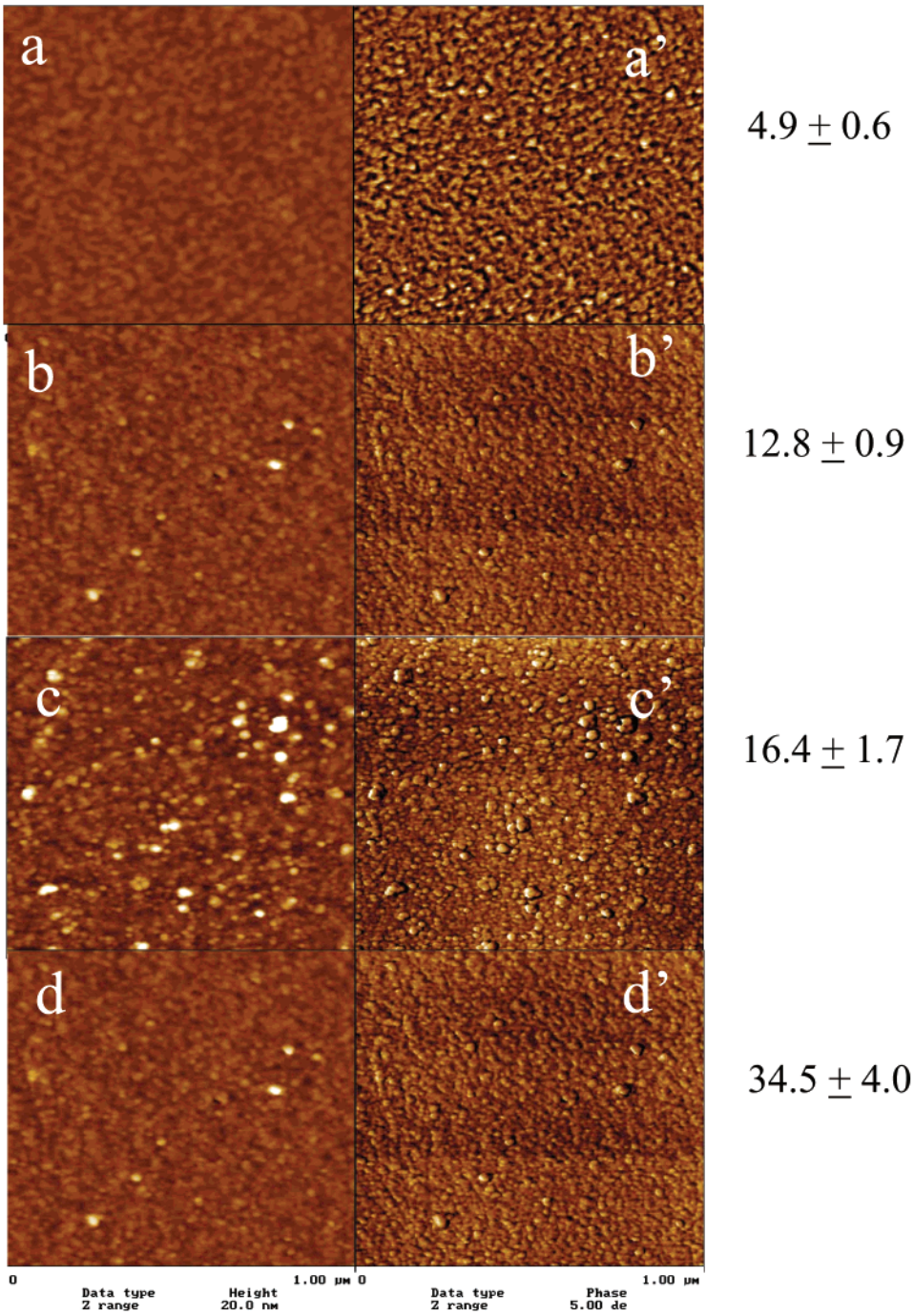

Figure 3. Representative AFM images of an Au surface coated with a 16-mercaptohexadecanoic acid SAM (a) before and (b) after treatment for 3 min with 0.006 mM $SnCl_2$ in a 50/50 mixture of water and methanol, (c) after treatment with 0.027 M ammoniacal $AgNO_3$, and (d) after treatment with electroless Au plating solution containing Au(I) and 0127 M formaldehyde.

morphology and composition of the junction. It is particularly important to prevent the plating of metal through pinholes in the monolayer, which would connect the two portions of the nanowires. To prevent this electrical shorting, an electroless plating procedure was used to plug pinholes before plating the second portion of the nanowires. This process involved reduction of Au(I) to Au(0) with formaldehyde as a reducing agent.[27] The reaction is catalyzed by Ag nanoparticles which are generated in situ from the reduction of Ag(I) by Sn^{2+} adorbed on top of the monolayer. This electroless plating procedure has been described in detail elsewhere.[27,35,36]

To characterize the morphology of the electrolessly plated layer, we used TEM, AFM, and XPS to examine the changes that occur as the top metal caps are generated through the "seeding" procedure.

AFM Experiments. These experiments were done on planar Au substrates, made with smooth evaporated Au. Figure 3a−d shows a series of representative AFM images as the Au surface

(35) Mallory, G. E.; Hajdu, J. B.; Eds. *Electroless plating: Fundamentals and applications*; American Electroplaters and Surface Finishers Society: Orlando, Fla. 1990.
(36) McDermott, J. *Plating of plastics with metals*; Noyes Data Corporation, NJ, 1974.

Table 1. XPS Analysis of Planar Au-Coated Substrates Treated with Mercaptohexadecanoic Acid and Taken through the Electroless Plating Procedure

sample	treatment	Au	O	C	S	N	Ag	Sn
I	C-16−SAM only[a]	19.3	7.0	69.4	3.4	1.9	0.0	0.0
II	C-16-SAM/Sn^{2+}	14.0	20.4	52.3	1.8	1.4	0.0	10.1
III	C-16-SAM/Sn^{2+}/Ag^{+}	9.6	34.1	39.5	0.9	0.5	3.0	7.1
IV	C-16-SAM /Sn^{2+}/Ag^{+}/Au^{+}	58.9	2.2	35.7	2.4	0.0	0.8	0.0
V	C-16-SAM/Sn^{2+}/Au^{+}	29.1	25.5	28.4	0.0	0.0	0.3	16.7

[a] C-16-COO^{-}.

is treated with a monolayer, then with Sn(II), Ag(I), and Au(I) solutions.[27]

The monolayer coated Au is essentially featureless (Figure 3a), and treatment with Sn(II) has little effect on the surface morphology as seen in Figure 3b. This can be seen from analysis of the mean surface roughness, Figure 3a−d. The mean surface roughness of the area shown in Figure 3a is 2.8 nm before treatment. Analysis of a smaller selected area (0.1 μm^2) gave a surface roughness of 0.48 nm. The global surface roughness for the area in Figure 3b was 5.6 and 0.6 nm for a 1 μm selected area that did not contain obvious large features.

A dramatic change in morphology occurs when the Sn(II) coated surface is treated with Ag(I), as seen in Figure 3c. Large features appear on the surface and the mean surface roughness increases to 16.1 nm for the imaged area and 1.3 nm for a smaller area. These large features are most likely nanoparticles of Ag, which are formed by reduction of Ag(I) by Sn(II). This suggests that upon reduction, Ag forms aggregates on the surface.

Figure 3d shows the AFM of the same surface after treatment with a solution of Au(I) with formaldehyde as a reducing agent. The surface roughness for the imaged area is 17.3 nm, while that of a selected 1 μm square area is 2.3 nm. From the phase contrast image, this surface is also more uniform in composition than any of the other surfaces. In control experiments, we established that omitting either the Sn or Ag step results in a patchy layer of Au.

XPS/FTIR Results. Film composition was established with XPS measurements as shown in Table 1. Combined with the AFM results, these data clearly demonstrate the importance of both Sn^{2+} and Ag^{+} in the seeding process. Table 1 also shows that most of the Sn remains on the surface and within the probe depth of XPS (1−2 nm) after Ag is deposited, consistent with the formation of Ag particles at low coverage. If the Ag particles are present, they catalyze the formation of a thick Au layer that covers the tin-oxide and Ag nanoparticles.

Surface reflectance IR of the films shows two main peaks in the high-frequency CH stretching region at 2856 and 2930 cm^{-1}. Both peaks are broadened, with shoulder peaks at 2851 and 2918 cm^{-1}. These spectra are consistent with the well-established formation of monolayers of thiols on Au surfaces.[37−40] The peak broadening and the high frequency of the CH_2 asymmetric stretch at 2930 cm^{-1} indicate that the presence of the terminal carboxylate group introduces some disorder into the SAM.

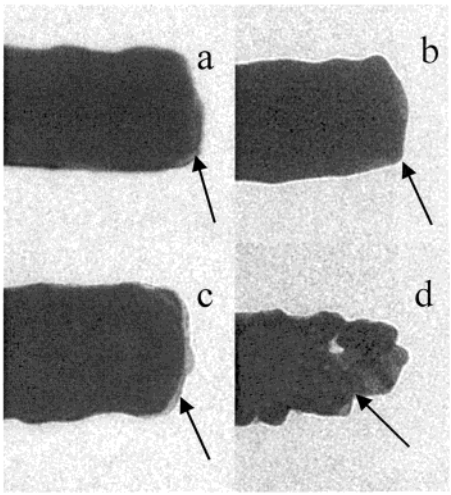

Figure 4. Representative TEM images of an Au surface coated with a mercaptohexadecanoic acid SAM (a) before and (b) after treatment for 3 min with 0.006 mM $SnCl_2$ in a 50/50 mixture of water and methanol, (c) after treatment with 0.027 M ammoniacal $AgNO_3$, and (d) after treatment with electroless Au plating solution containing Au(I) and 0127 M formaldehyde.

TEM Study of the Seeding Process. Figure 4a−d shows a series of TEM images of Au nanowires at various stages in the electroless seeding/plating process. Before treatment with Sn(II) the monolayer is not visible, as seen in Figure 4a. After treatment with Sn(II) solution, there is a slight enhancement in the contrast between the molecular layer and the Au portions of the nanowire (Figure 4b), most likely because of the presence of heavy elements. This contrast is greatly enhanced when the nanowires are treated with ammoniacal Ag(I) solution (Figure 4c). Sn(II) coordinates to the carboxyl groups at the top of the nanowires, forming a layer that also likely contains charge balancing chloride ions and water of hydration. Interestingly, the average thickness of the low-contrast layer from the TEM image in Figure 4c is 2−3 nm, which is in good agreement with the value measured by ellipsometry (2.4 ± 0.1 nm) for 16-mercaptohexadecanoic films on planar Au substrates.

A thick Au layer is formed when the nanowires are exposed to the electroless Au plating bath that contains formaldehyde as seen in Figure 4d. The very rapid formation of the Au is a result of the catalytic effect of Ag for the reduction of Au(I) to Au(0) and the autocatalytic effect of Au(0).

I−V Measurements. Individual Au and Au-16-mercaptohexadecanoic acid-Au nanowires were aligned between metal fingers on an insulating substrate. A scanning electron microscope (SEM) image of a Au-16-mercaptohexadecanoic acid-Au nanowire spanning the two photolithographically defined metal fingers is shown in Figure 5a. The 5.5 μm long nanowire is centered between the metal electrodes, with approximately 1 μm long segments of the nanowires contacting each of the fingers. Because the molecular junctions are placed near the center of the wire, they should be located in the gap between the electrode fingers. Figure 5b shows a lower magnification SEM image of the same device on the substrate illustrating the electrical contact between the nanowire and the large area, 100 × 100 μm^2, metal probe pads.

(37) Snyder, R. G.; Strauss, H. L. *J. Phys. Chem.* **1982**, *86*, 5145.
(38) Stranick, S. J.; Parikh, A. N.; Tao, Y. T.; Allara, D. L.; Weiss, P. S. *J. Phys. Chem.* **1994**, *98*, 7636.
(39) Dunbar, T. D.; Cygan, M. T.; Bumm, L. A.; McCarty, G. S.; Burgin, T. P.; Reinerth, W. A.; Jones, L., II; Jackiw, J. J.; Tour, J. M.; Weiss, P. S.; Allara, D. L. *J. Phys. Chem. B* **2000**, *104*, 5880.
(40) Tao, Y.-T.; Lin, W.-L.; Hietpas, G. D.; Allara, D. L. *J. Phys. Chem. B* **1997**, *101*, 9732.

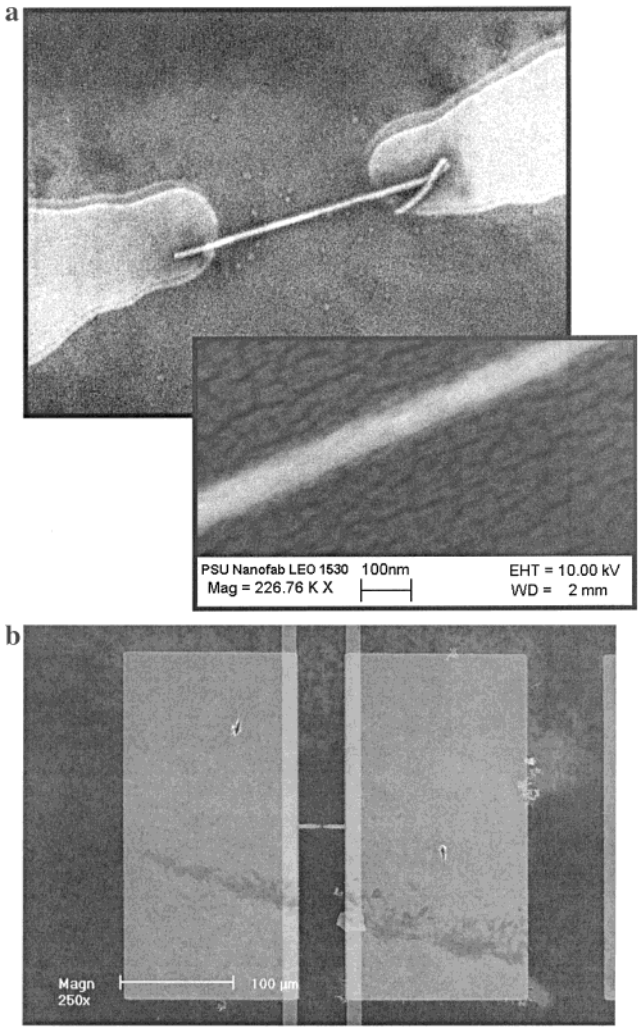

Figure 5. FESEM images of an Au-SAM-Au nanowire spanning the gap between Au contact electrodes (a) at high magnification and (b) at lower magnification showing the region making contact with the probe pads.

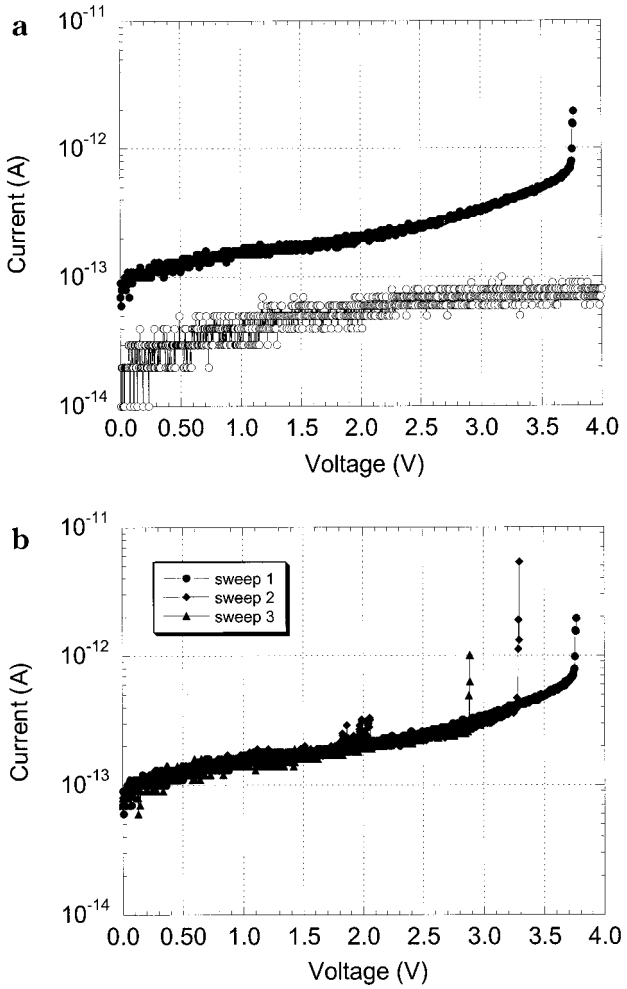

Figure 6. Current−voltage characteristics of a representative Au-SAM-Au nanowire connected to Au probe pads. (a) Fifth positive cycle after four cycles to 3.5 V; open circles show background current with no nanowire in the junction. (b) Progressive degradation of the I−V characteristics with repeated cycling to the breakdown voltage.

The contact resistance between the nanowire and the electrode fingers was determined by measuring the I−V properties of solid Au nanowires without molecular junctions. From these measurements, it was determined that the resistance of the electrode-nanowire contact and the metal nanowire was approximately 100 ohms, which results in 100 μA of current at 10 mV. This verifies that the contact between the nanowire and the metal electrode has very low resistance, and that it does not limit the current of Au-16-mercaptohexadecanoic acid-Au nanowire junctions.

Parts a and b of Figure 6 show semilogarithmic I−V plots for a nanowire containing a monolayer of 16-mercaptohexadecanoic acid between two Au segments. Figure 6a shows the I−V characteristics of the fifth positive cycle of the junction (filled circles), where the first four cycles were limited to a voltage less than 3.5 V. The I−V characteristics of the first four sweeps are not shown because they overlay these data exactly. This figure also includes a control measurement (open circles) in which the current was measured between the two metal electrodes with a 3 μm gap without a nanowire spanning the electrodes. This provides a measure of the background surface leakage current of the BCB dielectric, which is less than 10^{-13} A at a bias of 4 V.

The data in Figure 6a show that the low-bias current of the junction is a factor of 2 to 3 times the background leakage current of approximately 50 fA. At biases exceeding 2.0 V, the current increases more rapidly with voltage, exhibiting a nearly exponential dependence on voltage with a slope of approximately 0.29 decade/V for biases between 2.5 and 3.5 V. Finally, a sharp increase in current is observed at a bias of 3.55 V, reaching the current compliance of 10 pA at 3.6 V. Subsequent sweeps of the same molecular junction where the current compliance was limited to 10 pA are shown in Figure 6b. In each case, the low-bias region of the current did not change significantly; however, the critical bias at which breakdown occurred was reduced by approximately 0.3 V/cycle. Similar measurements were conducted on junctions fabricated during the same synthetic run, where the current compliance was increased from 10 to 100 pA. In contrast to the characteristics shown in Figure 6b, these junctions typically reached compliance at a bias less than 1V, showing that junction degradation occurs more rapidly when high current densities are permitted to flow through the SAM.

The I−V characteristics shown in Figure 6 are typical of those measured on nonshorted Au-16-mercaptohexadecanoic acid-Au nanowire junctions. These experiments were repeated on devices

fabricated during several synthetic runs and the range of breakdown voltages was found to vary from 2.8 to 3.7 V, with the largest fraction of the junctions having breakdown voltages between 3.5 and 3.8 V. A small number of the nonshorted devices had breakdown voltages near 7 V, which may be indicative of a multilayer SAM junction that formed in these nanowires during synthesis.

The I−V characteristics of metal-alkanethiol-metal junctions of varying chain length have been measured using several techniques, including CP-AFM[24,25] and liquid Hg-SAM-metal contacts.[26] These reports show that the dominant transport mechanism at low bias (ohmic region) is coherent nonresonant tunneling, where the decay constant β_n is exponentially dependent on chain length. Frisbie et al. reported that the average zero bias junction resistance increased by 1 order of magnitude per two carbons, yielding an average junction resistance of 2×10^{10} Ω for C-12.[24] On the basis of these published data, it appears that the simple nonresonant tunneling model cannot be extended to describe the I−V behavior of alkane junction at higher biases where the current increases exponentially with voltage. The breakdown voltage has also been studied for alkanethiol junctions of various chain lengths and probe contact forces. The breakdown field strength has been found to be relatively independent of molecular chain length and varies from 1 to 3.5×10^9 V/m, with the highest field strengths measured with a CP-AFM in a liquid controlled environment at low contact force. As the contact force on the monolayer was increased, the critical bias for breakdown was reduced. Lindsey et al. also reported enhanced conductivity on measurements of alkanethiol monolayers exceeding the critical breakdown bias. The enhanced conductivity was attributed to the electric field rather than a change in morphology (height) of the monolayer.[25]

The very small low-bias currents associated with our C-16 mercaptohexadecanoic acid junctions make it difficult to calculate accurately the zero-bias resistance of the molecular junction. However, after accounting for the background leakage current due to the measurement template, we estimate that the zero-bias resistance exceeds 10^{13} Ω. This value is 1 order of magnitude higher than what would be predicted by Frisbie et al. based on a C-16 monolayer.[24] However, our junction also has a contribution of resistance due to the carboxyl end group, which may account for the larger resistance.

At higher biases, we were not able to fit the exponential increase in current using a simple planar barrier nonresonant tunneling model over the large range of voltages for which our slope was constant.[41] It is not surprising that this model does not accurately predict the I−V dependence of the alkanethiol junction at higher biases because it does not take into account any of the more complex molecule-to-molecule interactions that may amplify tunneling current.[42] It is notable, however, that the magnitudes of the currents that we measure in this 2 nm thick Au-16-mercaptohexadecanoic acid-Au junction are comparable to the measured and simulated gate current density for a 2.1 nm thick SiO_2 gate oxide with a barrier height of 2.6 eV relative to the polysilicon gate.[43]

The rapid increase in current that corresponds to dielectric breakdown for the first sweep of the junction in Figure 6a occurs at a voltage of 3.6 V. If we assume a SAM thickness of 2 nm, this is equivalent to a breakdown field strength of 1.8×10^9 V/m. This is within the range of breakdown strengths measured by mercury contact and CP-AFM experiments. It was demonstrated by CP-AFM that the force on the SAM can impact substantially the critical bias for breakdown, leading to differences of up to 2 V decrease in critical bias as the force is increased by 8 nN.[24,25] In our experiments, we were not able to determine the force on the SAM experimentally. It is possible that the SAMs are either under tensile or compressive strain in nanowires that have been released from template membranes and aligned for measurement.

We observed a slow degradation in the critical bias for breakdown when the junction current exceeded 1 pA following junction turn-on, and a very rapid degradation when the junction current exceeded 100 pA. This suggests that only a fraction of the monolayer degrades when the maximum current at turn-on is limited, which constrains the overall power dissipation in the junction. However, when the current is not limited to such a small value, it is possible that a larger fraction (or the entire) SAM junction is impacted. At 100 pA current, the power dissipation in the junction is on the order of 10 W/cm^2, assuming that essentially all of the voltage drop occurs at the junction.

Conclusions

We have established the formation of a metal/SAM/metal junction inside nanowires through combined electroplating/electroless plating and template replication. This has been demonstrated by using a simple mercaptoalkanoic acid SAM, but the method is sufficiently general that the junctions could in principle be tailored to include a variety of electronically interesting molecules. This includes molecular wires with functional characteristics such as rectification and negative differential resistance. SAMs of these compounds could be prepared as a pure monolayer or mixed by insertion into defect sites of a carrier SAM such as 16-mercaptohexadecanoic acid. Thus, this method offers a new and simple way to impart interesting electronic characteristics to nanowires. It is also a relatively simple way to probe the electrical characteristics of molecules in the junction.

From TEM and X-ray diffraction data, we estimate the grain size of the Au nanowires to be on the order of 30 nm. Closely packed monolayers can have domains that extend over large areas, up to 50 nm^2. Thus, it is likely that there are defects within the SAMs studied here. However, the I−V measurements of transport in individual nanowires show that we can successfully seal pinholes in the SAM through the electroless seeding process. Our future efforts seek to characterize smaller diameter wires, which are less likely to contain defects, and to insert electronically active molecules in the SAMs to make functional nanowire devices.

Acknowledgment. We thank Dr. Rosemary Walsh and the Electron Microscope Facility for the Life Sciences in the Biotechnology Institute at Pennsylvania State University for the use of the transmission electron microscope, Dr. Ed Basgall of the Pennsylvania State Nanofabrication Facility for his assistance in taking FESEM images, and Josh Stapleton and Dr. David Allara for use of surface reflectance IR. This work was supported by DARPA and ONR under contract No. ONR-N00014-98-1-0846.

JA016696T

(41) Simmons, J. G. *J. Appl. Phys.* **1963**, *34*, 1793.
(42) Mujica, V.; Ratner, M. A. *Chem. Phys.* **2001**, *264*, 365.
(43) Lo, S. H.; Buchanan, D. A.; Taur, Y. *IBM J. Res. Dev.* **1999**, *43*, 3, 327.